6570 *Macromolecules* **2010**, *43*, 6570–6576
DOI: 10.1021/ma1011039

Macromolecules
ARTICLE

Stepwise Radial Complexation of Triphenylmethyliums on a Phenylazomethine Dendrimer for Organic−Metal Hybrid Assembly

Yousuke Ochi,[‡] Atunobu Fujii,[‡] Reina Nakajima,[‡] and Kimihisa Yamamoto*[,†]

[†]*Chemical Resources Laboratory, Tokyo Institute of Technology, Yokohama 226-8503, Japan, and*
[‡]*Department of Chemistry, Faculty of Science and Technology, Keio University, Yokohama 223-8522, Japan*

Received May 17, 2010; Revised Manuscript Received June 24, 2010

ABSTRACT: Dendritic polyphenylazomethine (**DPA**) stepwisely complexes with metal ions based on the interaction between a Lewis acid and base. **DPA** has π-conjugated rigid backbones, which are suitable for delocalization of cation charges. In this study, triphenylmethylium (TPM) could coordinate to the imine group of the fourth generation of **DPA** (**DPAG4**, **DPAG*X***, designated G*X*, where *X* is the generation number) in a stepwise radial fashion, which allows control of the number and position of TPM on a dendrimer as metal ions do. For the detailed investigation of TPM precise assembly, this paper have shown that **DPAG4-ZnP**, a porphyrin core phenylazomethine dendrimer having 60 imine sites, could complex with TPMs in a stepwise fashion similar to that of *p*-phenylene core **DPAG4** having 30 imine sites. In addition, the investigation of the hybrid assembly using TPM and metal ions on **DPAG4** was performed. We confirmed that the inner layer of **DPAG4** was complexed with TPM, followed by the outer layer with $SnCl_2$. This study developed the range of controlling precise assembly on a **DPA** mold. The process of TPM assembly was analyzed using UV−vis spectroscopy, NMR, free volume, and cyclic voltammetry.

Introduction

Dendrimers[1] are highly branched macromolecules which have a single molecular weight like proteins. They have been noted as a possible building block for fabricating new nanomaterials. These dendrimers contain a nanosized space in the center into which functional substances can be incorporated to give nanocapsules which can be used as drug delivery systems,[2] metal catalysts,[3] and dyes.[4] The well-defined structure and high density of surface functionalities may allow tuning of toxicity and release properties in DDS. The isolation effect of dendrimers prevents a self-aggregation or degradation of dyes, which would improve their properties. Although many researchers have investigated the encapsulation behavior of dendrimers via coordinative bonds,[3] ionic bonds,[5] or hydrophobic interactions,[6] it has been difficult to incorporate organic molecules quantitatively into the dendrimer due to a random statistical distribution. As one solution for that, we previously reported a novel method of precise assembly of metal ions on a dendritic polyphenylazomethine (**DPA**, Chart 1a), that is, a phenylazomethine dendrimer.[7]

Triphenylmethylium (TPM, Chart 1b) contains a carbocation stabilized by the delocalization over three phenyl rings. Triphenylmethylium is one of the most famous carbocations, which has been utilized for catalysts,[8] dyes,[9] redox activity,[10] and photoresponsive materials[11] and so on. The synthetic convenience of TPM allows the various molecular designs and conditions of the carbocation. Actually, various kinds of rhodamine derivatives were synthesized by a phenyl substitution. In addition, TPM has the property of Lewis acidity, which is famous for dehydration from cycloheptatriene. For the development of their catalytic ability, polymer or resin bounded TPMs have also been studied.[12] Otherwise, Müllen's group reported the polyphenylene dendrimers incorporating trityl groups on its phenyl backbone to stabilize their charge/spin.[13] TPM is a fundamental and attractive backbone for the creation of various functional materials.

*Corresponding author. E-mail: yamamoto@res.titech.ac.jp. Telephone: +81(45)924-5260.

Chart 1. Structure of (a) the Fourth Generation of Dendritic Polyphenylazomethine (DPAG4) and (b) Triphenylmethylium Tetrafluoroborate ((TPM)BF_4)

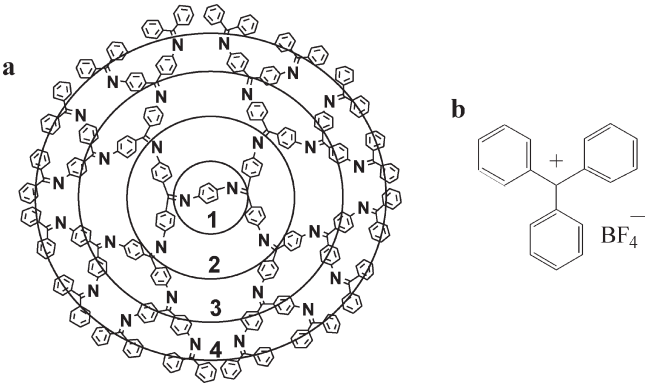

DPA could assemble various kinds of metal ions based on the interaction between metal Lewis acids and **DPA** imines. In addition, **DPA**'s π-conjugated dendritic structure is suitable for the delocalization of cation charges. In this study, precise assembly of an organic Lewis acid, TPMs, on **DPA** was demonstrated. In contrast to metal-ion assembly, the incorporation of organic species allows for application of the resulting species in the formation of new nanomaterials, taking advantage of the flexibility and functionality. We found that TPM could be coordinated to the imine group of **DPA** in stepwise radial fashion, which allows for control of the number and position of TPMs incorporated into a dendrimer. For a detailed investigation of TPM precise assembly, this paper reports that **DPAG4-ZnP** having 60 imine sites could complex with TPM in a fashion similar to a *p*-phenylene core **DPAG4** having 30 imine sites. In addition, the hybrid assembly using TPM and metal ions on a **DPAG4** was performed. The variation in controlling a precise assembly on a **DPA** mold was developed using TPM.

 Published on Web 07/21/2010

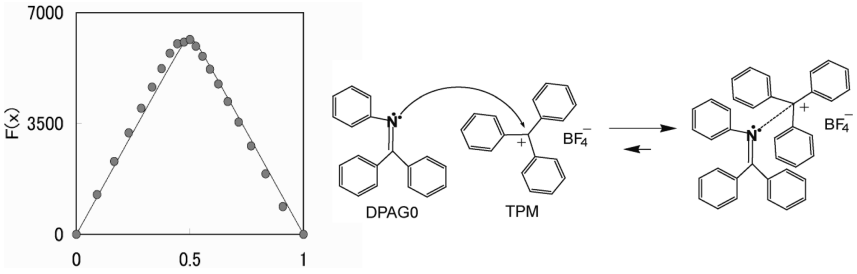

Figure 1. A Job plot[18] of (TPM)BF_4 and **DPAG0**. $F(x) = \text{Abs}/(C_{G0} + C_{TPM^+BF_4^-}) - (\varepsilon_{G0} - \varepsilon_{TPM^+BF_4^-})x - \varepsilon_{TPM^+BF_4^-}$, $x = C_{G0}/(C_{G0} + C_{(TPM)BF_4})$; units molar fraction of **DPAG0**. Chloroform/acetonitrile (1/1) solution of **DPAG0** and (TPM)BF_4 with the same concentration, 2.5×10^{-4} M, were mixed in various proportions. The plot shows a maximum at a 0.5 mol fraction of **DPAG0**. The equilibrium constant of complexation, *K*, obtained by curve-fitting a theoretical simulation to the experimental data was 5×10^6 M^{-1}.

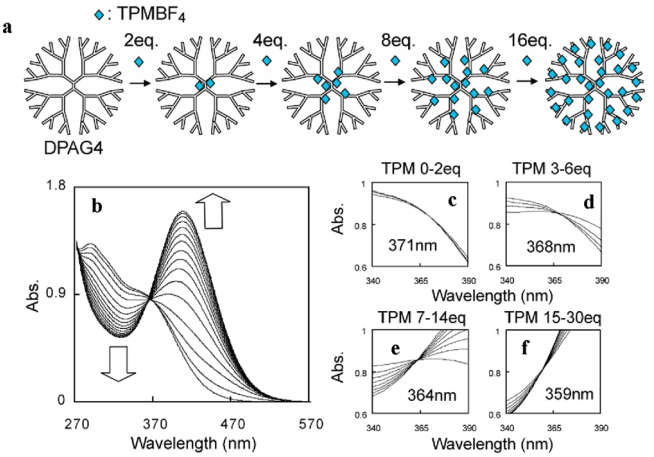

Figure 2. (a) Schematic representation of the stepwise radial complexation of **DPAG4** with (TPM)BF_4. (b) UV−vis spectra of **DPAG4** 0−30 equiv of (TPM)BF_4 and isosbestic points during the addition of (c) 0−2, (d) 3−6, (e) 7−14, and (f) 15−30 equiv of (TPM)BF_4. [**DPAG4**] = 5.0×10^{-6} M.

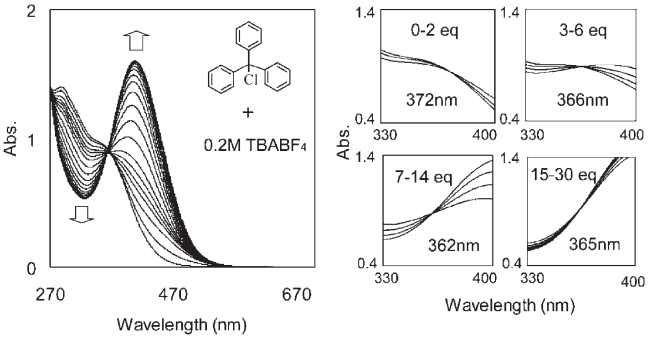

Figure 3. UV−vis spectra of **DPAG4** complexed with 30 equiv of (TPM)Cl in $CHCl_3/CH_3CN$ = 1/1 solution with 0.2 M (TBA)BF_4. [**DPAG4**] = 5.0×10^{-6} M.

Results and Discussion

UV−Vis Spectroscopy. A triphenylmethylium (TPM) carbocation can coordinate to a pyridine nitrogen atom.[14] Previously, we reported the association of Rhodamine 6G on **DPA**, which include a structure similar to TPM.[15] In this study, the stepwise complexation behavior between triphenylmethylium tetrafluoroborate ((TPM)BF_4) and DPA was observed by UV−visible spectroscopy during a titration in which (TPM)BF_4 was added to the imine sites of **DPAG4** having 30 imine sites. It was observed that the absorption around 445 nm increased while the absorption around 310 nm attributed to the imines decreased (Figure 1a). This behavior resembled that of the stepwise complexation between an imine and a metal salt, such as $FeCl_3$[16] or $SnCl_2$.[17] A Job plot[18] showed that **DPAG0** (Chart S1a, Supporting Information) forms a 1:1 complex with (TPM)BF_4 (Figure 1). The disappearance of yellow color (λ_{max} = 405 and 435 nm) attributed to the TPM carbocation on adding DPAG0 also confirmed the complexation.[19]

Stepwise radial complexation based on the electron gradient, which was due to electron-donating imines forming the dendritic skeleton.[20] Stepwise radial complexation of (TPM)BF_4 on **DPAG4** (Figure 2a) was confirmed by UV−vis spectroscopy. An isosbestic point appears when one compound is quantitatively transformed into another by complexation (see Supporting Information). Four changes in the position of the isosbestic points were observed during the addition of (TPM)BF_4 to **DPAG4**, which indicated that four different complexations are successively formed upon (TPM)BF_4 addition (Figure 2b). These shifts are very similar to those observed during complexation of metal ions. The spectra of **DPAG4** changed gradually with an isosbestic point at 371 nm observed up to the addition of 2 equiv of (TPM)BF_4 (Figure 2c) but shifted to 368 nm between 3 and 6 equiv (Figure 2d). During the addition of 7−14 equiv, an isosbestic point appeared at 364 nm (Figure 2e), which moved to 359 nm (Figure 2f) during the addition of 15−30 equiv. The number of equivalents of (TPM)BF_4 required to induce a shift was commensurate with the number of imine sites present in each generation layer of **DPAG4**. Similar stepwise complexations were observed in the cases of **DPAG2** and **DPAG3** (Figure S1). For **DPAG2**, two isosbestic points appeared at 343 and 360 nm when adding 0−2 and 3−6 equiv of (TPM)BF_4. In the case of **DPAG3**, three isosbestic points centered at 373, 361, and 355 nm appeared when adding 0−2, 3−6, and 7−14 equiv of (TPM)BF_4, respectively.

A triphenylmethylium can hold various kinds of counteranion, such as Cl, Br, BF_4, PF_6 and so on, which influence the ionization or stability.[10a] Different from metal salt cases, the TPM complexation with an imine requires the dissociation of a counterion from a carbocation to make an unoccupied orbital and to become a counterion of a TPM/**DPA** complex. In the case of a **DPA** complex, BF_4 was found to be suitable for a stepwise radial complexation and TPM halides ((TPM)Cl, (TPM)Br) did not allow a stepwise complexation. Although the UV−vis titration of TPM halides on **DPAG4** showed the change in the spectra, the shift of an isosbestic point was not observed because of the red shift (Figure S2). $TPMPF_6$ showed the complexation but the change was relatively small due to a weak complexation constant. However, the condition of excess BF_4 allows the stepwise radial complexation of TPM halides. UV−vis titration of (TPM)Cl in 0.2 M (TBA)BF_4 solution was performed. The four shifts of isosbestic points showed that a stepwise radial complexation of (TPM)Cl had occurred in 0.2 M (TBA)BF_4 solution (Figure 3), which was

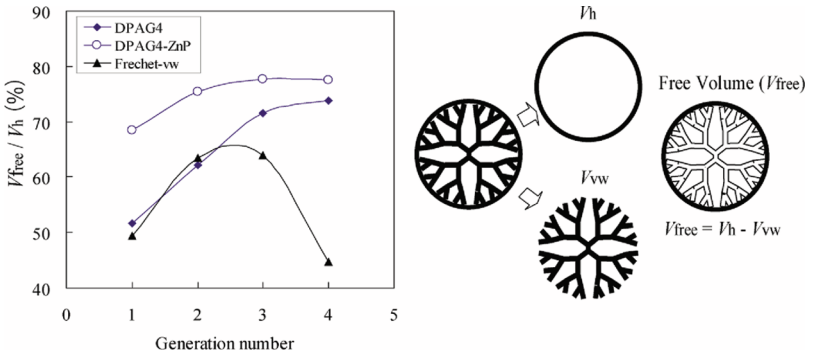

Figure 4. Free volume ($V_{free} = V_h - V_{vw}$) of **DPAG4**, **DPAG4-ZnP** and a Fréchet-type dendrimer. The figure shows the rate of free volumes (V_{free}/V_h) of each generation of dendrimers. The van der Waals volumes are referred to and calculated based on previous studies.[22]

Table 1. Hydrodynamic Volume (V_h), van der Waals Volume (V_{vw}), and Free Volume (V_{free}) of each Dendrimer[a]

dendrimer	V_h (Å^3)	V_{vw} (Å^3)	V_{free} (Å^3)	$V_{(TPM)BF_4}$ (Å^3)	V_{free}'[b] (Å^3)	V_{free}'/V_h (%)
DPAG4	18557	4583	13704	8133	5571	30
DPAG4-ZnP	44889	10095	34794	16265	18529	41

[a] V_{free}' means the free volume of the (TPM)BF_4 full complexed dendrimer. [b] $V_{free}' = V_{free} - V_{(TPM)BF_4}$.

caused by the exchange of the counteranions, Cl to BF_4. Similarly, (TPM)Br could complex stepwisely under the condition of 0.1 M (TBA)BF_4 (Figure S3). These results suggest that BF_4 stabilize a stepwise TPM complexation. If TPM derivatives were difficult to isolate BF_4 salts because of synthetic difficulty, TPM halides under an excess BF_4 condition will allow a stepwise complexation.

NMR Analysis. The complexation of **DPA** with (TPM)-BF_4 was observed using ^{1}H NMR and ^{13}C NMR spectra (Figure S4). The carbon peak of the imine site (C_1, **DPAG0**) shifted from 167 to 179 ppm on addition of an equimolar amount of (TPM)BF_4 (Figure S4B). This is probably because of the decrease in the π electron density of the imine site due to the complexation. After the complexation, a new peak appeared at 81 ppm, this was identified as the quaternary carbon of TPM coordinated to the nitrogen of imine (C_2), which corresponded to the neutralization of the TPM carbocation by a **DPA** imine. The number of peaks for the complex was equal to the sum of the peaks of **DPAG0** and TPM. Comparison of the ^{1}H NMR spectra of **DPAG0** with that of **DPAG0** after the addition of an equimolar amount of (TPM)BF_4 showed that all the peaks of the **DPAG0** shifted downfield due to the electron withdrawing effect of (TPM)BF_4 (Figure S4A). In addition, Figure S4C shows the molecular modeling of **DPAG0** and TPM using MOPAC-AM1. A similar structure was reported in the X-ray crystal structure analysis of the $(C_6F_5)_3B$/imine complex,[21] which supports the idea that the steric hindrance between a **DPA** imine and a three aryl unit would not become a problem in the complexation.

Free Volume in a DPA. (TPM)BF_4 can be trapped in DPA because the **DPA** skeleton is rigid and has sufficient space to incorporate molecules, although (TPM)BF_4 has a larger molecular size than metal salts. For discussing about the free space, the free volume in a dendrimer (V_{free}) was calculated based on the difference between van der Waals volume V_{vw}[22] and the hydrodynamic volume (V_h) using the hydrodynamic radius in THF detected by SEC. According to this calculation, the rate of free volume (V_{free}/V_h) of **DPAG4** and a porphyrin core **DPAG4** (**DPAG4-ZnP**) were determined to be 74% and 78%, respectively,[23] which were much larger than that of a Fréchet type G4 dendrimer, 45% (Figure 4).[24] In addition, Table 1 shows that the free volume rate of **DPAG4** complexed with 30 equiv of (TPM)BF_4 (V_{free}'/V_h) would be reduced to 30%. The free volume rate of **DPAG4-ZnP** having 60 imine sites complexed with 60 equiv of (TPM)BF_4 would be reduced to 41% (Table 1), which are larger than that of a Fréchet type G4 dendrimer in DMF (21%).[24] These results support that the fully stepwise radial complexation of TPM^+ and BF_4^- into a phenylazomethine dendrimer was possible in terms of the free space in a dendrimer.

Porphyrin Core DPA. Zinc porphyrin core **DPA**, that is, **DPAG4-ZnP** (Figure 5a), has 60 imine sites; that is, each layer has double the number of imines compared to the *p*-phenylene core **DPA**, 4, 8, 16, and 32, respectively.[25] As suggested by the discussion of the free volume, the stepwise radial complexation of (TPM)BF_4 on **DPAG4-ZnP** (Figure 5b) was confirmed by UV−vis spectroscopy. Four changes in the position of the isosbestic points were observed during the addition of (TPM)BF_4 to **DPAG4-ZnP**, which indicated that four different complexations are successively formed upon (TPM)BF_4 addition (Figure 5c). The spectra of **DPAG4-ZnP** changed gradually with an isosbestic point at 373 nm observed up to the addition of 4 equiv of (TPM)BF_4 but shifted to 369 nm between 5 and 12 equiv. During the addition of 13−28 equiv, an isosbestic point appeared at 362 nm, which moved to 356 nm during the addition of 29−60 equiv. The number of equivalents of (TPM)BF_4 required to induce a shift was commensurate with the number of imine sites present in each generation layer of **DPAG4-ZnP**, 4, 8, 16, and 32, respectively. Similar stepwise complexations were also observed for **DPAG3-ZnP**, **DPAG2-ZnP** and **DPAG1-ZnP** (Figure S5). In the case of **DPAG3-ZnP**, three isosbestic points centered at 367, 365, and 356 nm appeared when adding 0−4, 5−12, and 13−28 equiv of (TPM)BF_4, respectively. For **DPAG2-ZnP**, two isosbestic points appeared at 343 and 360 nm when adding 0−4 and 5−12 equiv of (TPM)BF_4. **DPAG1-ZnP** has only four imines, so that one isosbestic point was observed at 443 nm. The numbers of (TPM)BF_4 equivalents which were required to induce a shift agreed with the number of imine sites present in each generation layer of **DPAG4-ZnP**, 4, 8, 16, and 32, which confirmed a stepwise radial complexation similar to that **DPAG4**.

Electrochemical Analysis. The zinc porphyrin core shows reversible redox waves on a cyclic voltammogram. We observed the redox wave characterized as a $1e^-$ oxidation to the monocation radical (ZnP^+). The redox potential of the zinc porphyrin ring clearly shows the effect by *meso*-substitution. Actually the stepwise complexation of metal salts on **DPA-ZnP**

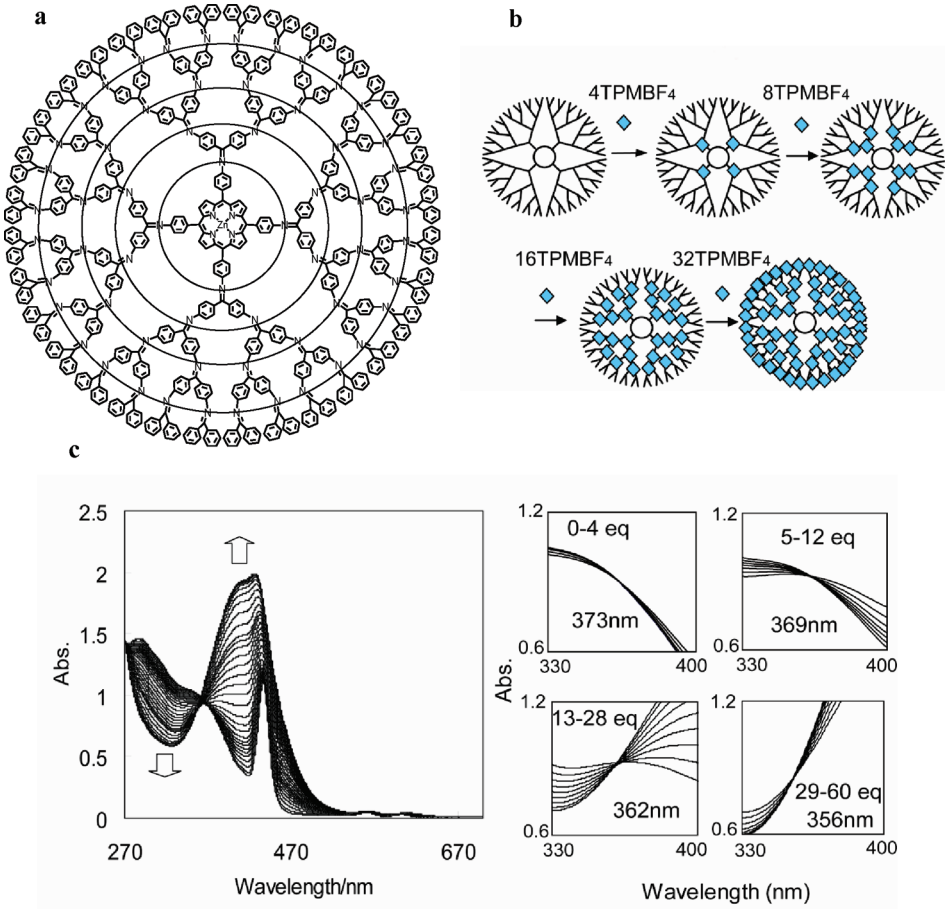

Figure 5. (a) Structure of **DPAG4-ZnP**. (b) Schematic representation of the stepwise radial complexation of **DPAG4-ZnP** with $(TPM)BF_4$. (c) UV−vis spectra of **DPAG4-ZnP** 0−30 equiv of $(TPM)BF_4$ and isosbestic points during the addition of 0−4, 5−12, 13−28, and 29−60 equiv of $(TPM)BF_4$. [**DPAG4-ZnP**] = 2.5×10^{-6} M.

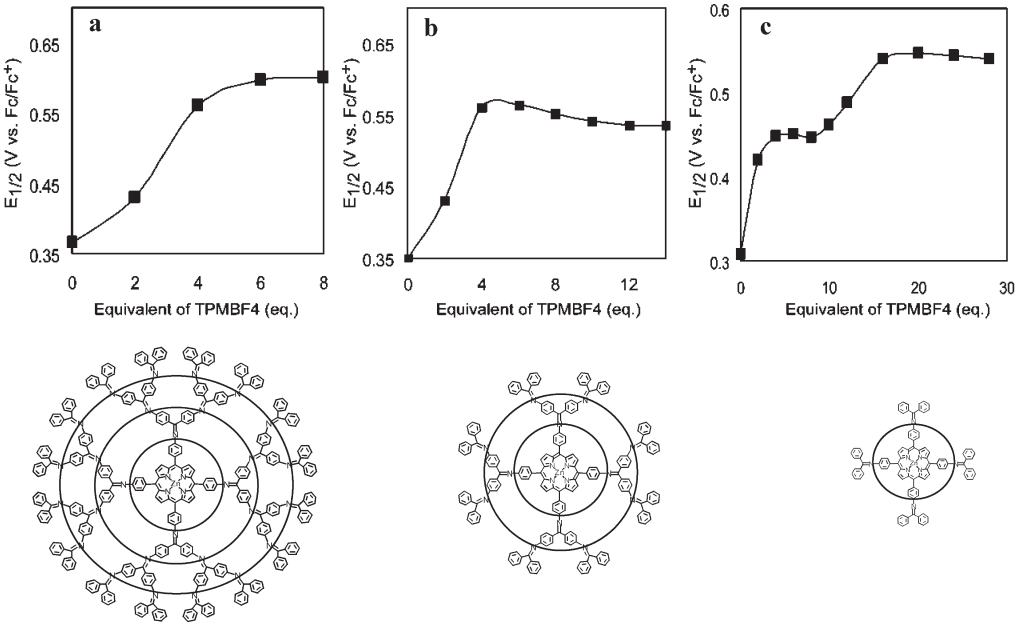

Figure 6. Changes in the redox potentials of (a) **DPAG3-ZnP** and (b) **DPAG2-ZnP** and **DPAG1-ZnP** complexed with $(TPM)BF_4$ measured by cyclic voltammetry. This positive shift on the addition of $(TPM)BF_4$ is attributed to the coordination of $(TPM)BF_4$ to the four inner imines, which involves an electron withdrawal effect through covalent bonds.

was analyzed using electrochemical method in a previous report.[25] Therefore, a zinc porphyrin core dendrimer could probe the stepwise assembly of TPM an electrochemically.

For **DPAG1-ZnP**, the observed half-wave potentials, middle value of the anodic and cathodic peak: $E_{1/2} = (E_{pa} + E_{pc})/2$) of the ZnP/ZnP^+ redox couple, positively shifted by 0.2 V after

full complexation of $(TPM)BF_4$ (Figure 6a). The redox potential shift occurred up to full complexation of the four molar amounts of $(TPM)BF_4$ to four imine units involving electron withdrawing through covalent bonds. This result was very similar to the behavior previously observed for a metal salt complex under the same conditions.[23] It was estimated that the Hammett constant was almost the same as that of the $FeCl_3$ complex ($\delta = 0.55$). The redox potential did not change when $(TPM)BF_4$ was added to *meso*-tetraphenyl zinc porphyrin without DPA imines. Thus, the addition of $(TPM)BF_4$ results in lowering of the electron density of the dendrimer core through the complexation with the imine sites of the dendrimer.

A reversible redox wave of the free base **DPAG2-ZnP** at 0.35 V was also shifted to a more positive value 0.54 V (vs Fc/Fc^+) by the coordination of $(TPM)BF_4$. The potential shift almost converged with four molar amounts of $(TPM)BF_4$ addition, although the number of imine sites is 12 (Figure 6b). The shift width almost agreed with that observed in the case of **DPAG1-ZnP** (+0.2 V). If the complexation was random, the redox potential would increase up to the addition of 12 molar amounts of $(TPM)BF_4$. This result shows the stepwise complexation from the first layer of imines.

On addition of 4 equiv of $(TPM)BF_4$ to **DPAG3-ZnP**, the redox potential of ZnP/ZnP^+ at the core shifted from 0.31 V (vs Fc/Fc^+) to 0.45 V (vs Fc/Fc^+). After the convergence of the first shift of the redox potential, it shifted to 0.55 V (vs Fc/Fc^+) again with the addition of 24 equiv of $(TPM)BF_4$, which is probably due to the environmental change around the porphyrin core by the complexation (Figure 6c). This stepwise behavior was very similar to the previously observed behavior for the $FeCl_3$ complex[25] (Figure S6). In addition to the **DPAG3-ZnP** experiments, we tried that of **DPAG4-ZnP** but it was difficult to detect $E_{1/2}$ from the broadened peak because of the decrease in the diffusion constant and the low solubility. However, a similar behavior like that of **DPAG3-ZnP** would seem to occur in the $FeCl_3$ case. In each ZnP core dendrimer, the redox shift behavior is related to the stepwise complexation of $(TPM)BF_4$, which was also confirmed by the UV−vis titration method.

Organic−Metal Hybrid Assembly on DPAG4. An organic−metal hybrid assembly could be achieved by taking advantage of the difference in the complexation constant to **DPA** imines, K ($K_{Fe} > 10^8$ M^{-1}, $K_{TPM} = 5 \times 10^6$ M^{-1}, $K_{SnCl_2} = 1.4 \times 10^4$ M^{-1}). In the previous study, we reported that heterometal assembling on **DPA** appears to be governed by the complexation ability of the metal salts, with a stronger coordinating metal in the inner layer and weaker coordinating metals in the outer layer.[26] The complexation abilities of $FeCl_3$, $SnCl_2$ and $(TPM)BF_4$ were compared by the normalized titration curve of **DPAG1** in $THF/CH_3CN = 1/1$ solution (Figure S7), which showed the faster convergence of $FeCl_3$ than that of $(TPM)BF_4$. These results confirmed that the order of complexation ability was as follows: $FeCl_3 > (TPM)BF_4 > SnCl_2$.

We demonstrated UV−vis titration by the addition of $FeCl_3$ followed by $(TPM)BF_4$ using **DPAG4** (Figure S8). After adding 14 equiv of $FeCl_3$, the isosbestic points were observed at 372 nm for 0−2 equiv of $FeCl_3$, 370 nm for 3−6 equiv, and 366 nm for 7−14 equiv, which correspond to the complexation of the first−third layers. After adding $(TPM)BF_4$, the isosbestic points shifted to 362 nm for 0−16 equiv of $(TPM)BF_4$, which corresponded to the complexation with the fourth layer. It was confirmed that the inner layer of **DPAG4** was complexed with $FeCl_3$, followed by the outer layer with $(TPM)BF_4$. Table S1 summarizes the isosbestic points for other adding patterns.

UV−vis titration by the addition of $(TPM)BF_4$ followed by $SnCl_2$ was also performed (Figure 7, and Table S1). After

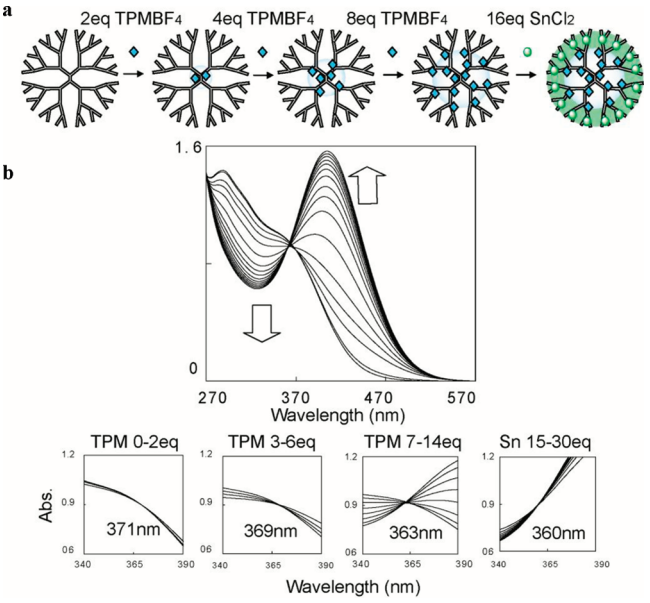

Figure 7. (a) Schematic representation of the hybrid complexation of **DPAG4** with $(TPM)BF_4$ and $SnCl_2$. (b) UV−visible spectra of **DPAG4** complexed with 14 equiv of $(TPM)BF_4$ followed by 16 equiv of $SnCl_2$ and isosbestic points during addition of $(TPM)BF_4$ and $SnCl_2$. [**DPAG4**] = 5.0×10^{-6} M.

adding 14 equiv of $(TPM)BF_4$, the isosbestic points were observed at 371 nm for 0−2 equiv of $(TPM)BF_4$, 369 nm for 3−6 equiv, and 363 nm for 7−14 equiv, which correspond to the complexation of first−third layers. After that, the isosbestic point shifted to 360 nm for the following 0−16 equiv of $SnCl_2$, which means the complexation with the fourth layer. In addition, in the case of the addition of $SnCl_2$ followed by $(TPM)BF_4$, the shift in isosbestic points was different from that of $(TPM)BF_4$ followed by $SnCl_2$. Figure S9 shows that $(TPM)BF_4$ complexes with the inner layer imines regardless of the order of their addition. Although the stepwise metal assembly on **DPAG4** usually occurs from the inner layer, the hybrid complexation using $(TPM)BF_4$ allows metal ions to complex with the outer layer selectively. This unique method gives **DPA** the more precise control of metal assembly on its π-conjugated backbone than before.

Conclusion

This study developed the variation in assembling species from metal ions to organic species. The organic cation, $(TPM)BF_4$, was found to complex with **DPA** in a stepwise fashion similar to that of metal ions. This stepwise radial complexation of TPM cations, which is assisted by BF_4 anions, suggests that DPA be suitable structure for delocalization of cation charges. Surprisingly, in addition to **DPAG4**, **DPAG4-ZnP** having 60 imines also could trap TPMs effectively in a stepwise fashion, due to its rigid skeleton having sufficient space. Considering that TPM can be easily tuned to Lewis acidity by phenyl substitution, an investigation of the quantitative assembly of various dyes based on a TPM skeleton is expected. If TPM derivatives were difficult to isolate as BF_4 salts, TPM halides under an excess BF_4 condition will allow a detailed analysis of the complexation behavior of TPM derivatives. Furthermore, the control of the number and location of metal ions on a DPA could be developed through the hybrid assembly of metals and TPMs. This hybrid complexation using $(TPM)BF_4$ enables metal ions to complex with the DPA outer layer selectively, which expands the variety of stepwise metal assembly using **DPA**. By expanding the range of molecules which are able to be encapsulated in DPA from metal ions to organic

molecules, we have taken an advanced step toward the design of novel nanomaterials.

Experimental Section

Methods. The UV−vis spectra were recorded using a Shimadzu UV-3100PC spectrometer with a sealed quartz cell (optical path length: 1 cm) at 20 °C. The details of the UV−vis titration method are described in the section General Method of UV−Vis Titration below.

The NMR spectra were recorded using a JEOL JMN400 FT-NMR spectrometer operating at 400 MHz (^{1}H) or 100 MHz (^{13}C). in $CDCl_3$:CD_3CN = 1:1 solvent + TMS solution. The ^{1}H NMR chemical shifts were referenced to the solvent peak ($CDCl_3$: 7.26 ppm) and tetramethylsilane (TMS: 0 ppm) as internal standards. The ^{13}C NMR chemical shifts were referenced to the solvent peak ($CDCl_3$: 77.0 ppm).

Cyclic voltammograms were recorded using an ALS 440 electrochemical analyzer. A glassy carbon electrode was used as the working electrode (φ = 3 mm), which was polished with 0.05 mm alumina paste before the analysis. The counter and the reference electrodes are Pt wire and Ag/Ag^+. All measurement was carried out with same Ag/Ag^+ reference after N_2 bubbling for 5 min. The measurement solution was 2 mL of $CHCl_3$:CH_3CN = 4:1 including 0.1 M $(TBA)PF_6$. The redox potential was then referenced to the ferrocene/ferrocenium standard by the half-wave potential of 0.2 mM ferrocene measured in 0.1 M Bu_4NClO_4/CH_3CN. The concentration of **DPAG*X*** (***X*** = 1−3) in each solution is 0.25 mM, followed by addition of $(TPM)BF_4$ acetonitrile solution.

Analytical size-exclusion chromatography (SEC) was performed using an HPLC (Shimazu, LC-10AP) equipped with a TSK-GEL CMHXL (Tosoh). Tetrahydrofuran (THF) was used as the eluent at the flow rate of 1 mL/min. The detection line was connected to a triple detector (Viscotek, TriSEC model 302).

The semiempirical molecular orbital calculation and optimizations of the molecular conformation were done on a Cache Worksystem ver. 5.04 (Fujitsu) employing the MOPAC-AM1 parameter.

Chemicals. All DPAs were synthesized by a previously reported method.[25,27] Triphenylmethylium tetrafluoroborate ($(TPM)BF_4$) and TPM halides were purchased from Tokyo Chemical Industry Co. Dehydrated chloroform and $SnCl_2$ were purchased from Wako Pure Chemical Industries; dehydrated acetonitrile were purchased from Kanto Kagaku Co. Dehydrated $FeCl_3$ and $(TBA)BF_4$ were purchased from the Kanto Kagaku Co.

General Method of UV−Vis Titration. Solutions of **DPAG4** (chloroform/acetonitrile = 1/1, 5.0×10^{-6} M), $(TPM)BF_4$ (acetonitrile, 5.0×10^{-3} M) were prepared in volumetric flasks. To a quartz cell was added 3.0 mL of the **DPAG4** solution, followed by the addition of 3 μL of $(TPM)BF_4$ solution (i.e., 1 equiv for **DPAG4**). The UV−vis spectra were measured until agreement was obtained with the one immediately before. Measurements were repeated after each addition of 3 μL of TPM solution to achieve UV−vis titration. After the measurement of UV−vis spectra, the absorption of $FeCl_3$ was subtracted to find the DPA absorption changes and isosbestic points.[16]

Acknowledgment. This work was supported by Grants-in-Aid for Scientific Research (Nos. 19205020, 21750152) and an Innovative Area (Coordination Programming, Area 2107, No. 21108009) from the Ministry of Education, Culture, Sports, Science and Technology, Japan, Mitsubishi and Futaba Foundation. Yousuke Ochi was supported by the "Doctor-21" scholarship program of Yoshida Scholarship Foundation and Keio Leading-edge Laboratory of Science and Technology Research Grant for Ph. D Program. We also thank Dr. T. Imaoka and Mr. K. Albrecht for their useful suggestion.

Supporting Information Available: Chart showing structures, text discussing the determination of the isosbestic point with a table, and figures showing additional UV−vis spectra, NMR, molecular modeling views, CV data, and titration curves. This material is available free of charge via the Internet at http://pubs.acs.org.

References and Notes

(1) (a) Newkome, G. R.; Yao, Z. Q.; Baker, G. R.; Gupta, V. K. *J. Org. Chem.* **1985**, *50*, 2003–2004. (b) Grayson, S. M.; Fréchet, J. M. J. *Chem. Rev.* **2001**, *101*, 3819–3868. (c) Tomalia, D. A.; Baker, H.; Dewald, J.; Hall, H.; Kallos, G.; Martin, S.; Roeck, J.; Ryder, J.; Smith, P. *Polym. J.* **1985**, *17*, 117–132. (d) Bosman, A. W.; Janssen, H. M.; Meijer, E. W. *Chem. Rev.* **1999**, *99*, 1665–1668.

(2) Ambade, A. V.; Savariar, E. N.; Thayumanavan, S. *Mol. Pharmaceutics* **2005**, *2*, 264–272.

(3) Crooks, R. M.; Zhao, M.; Sun, L.; Chechik, V.; Yeung, L. K. *Acc. Chem. Res.* **2001**, *34*, 181–190.

(4) (a) Arunkumar, E.; Forbes, C. C.; Smith, B. D. *Eur. J. Org. Chem.* **2005**, 4051–4059. (b) Froehling, P. E. *Dyes Pigm.* **2001**, *48*, 187–195. (c) Furuta, P.; Fréchet, J. M. J. *J .Am. Chem. Soc.* **2003**, *125*, 13173–13181. (d) Freeman, A. W.; Koene, S. C.; Malenfant, P. R. L.; Thompson, M. E.; Fréchet, J. M. J. *J. Am. Chem. Soc.* **2000**, *122*, 12385–12386.

(5) (a) Ornelas, C.; Boisselier, E.; Martinez, V.; Pianet, I.; Aranzaes, J. R.; Astruc, D. *Chem. Commun.* **2007**, *47*, 5093–5095. (b) Cooke, G.; Sindelar, V.; Rotello, V. M. *Chem. Commun.* **2003**, *6*, 752–753.

(6) (a) Morgan, M. T.; Carnahan, M. A.; Immoos, C. E.; Ribeiro, A. A.; Finkelstein, S.; Lee, S. J.; Grinstaff, M. W. *J. Am. Chem. Soc.* **2003**, *125*, 15485–15489. (b) Kojima, C.; Kono, K.; Maruyama, K.; Takagishi, T. *Bioconjugate Chem.* **2000**, *11*, 910–917.

(7) Yamamoto, K.; Higuchi, M.; Shiki, S.; Tsuruta, M.; Chiba, H. *Nature* **2002**, *415*, 509–511.

(8) (a) Chen, C. T.; Chao, S. D.; Yen, K. C.; Chen, C. H.; Chou, I. C.; Hon, S. W. *J. Am. Chem. Soc.* **1997**, *119*, 11341–11342. (b) Tao, T.; Maciel, G. E. *Macromolecules* **1997**, *30*, 8826–8232. (c) Denmark, S. E.; Chen, C. T. *Tetrahedron Lett.* **1994**, *35*, 4327–4330. (d) Shchepinov, M. S.; Korshun, V. A. *Chem. Soc. Rev.* **2003**, *32*, 170–180.

(9) (a) Malpert, J. H.; Grinevich, O.; Strehmel, B.; Jarikov, V.; Mejiritski, A.; Neckers, D. C. *Tetrahedron* **2001**, *57*, 967–974. (b) Hojo, M.; Ueda, T.; Yamasaki, M.; Inoue, A.; Tokita, S.; Yanagita, M. *Bull. Chem. Soc. Jpn.* **2002**, *75*, 1569–1576.

(10) (a) Hojo, M.; Hasegawa, H.; Tsurui, H.; Kawamura, K.; Minami, S.; Mizobe, A. *Bull. Chem. Soc. Jpn.* **1998**, *71*, 1619–1627. (b) Rathore, R.; Burns, C. L.; Guzei, I. A. *J. Org. Chem.* **2004**, *69*, 1524–1530.

(11) (a) Jiang, Y.; Wang, Y.; Ma, N.; Wang, Z.; Smet, M.; Zhang, X. *Langmuir* **2007**, *23*, 4029–4034. (b) Miyagawa, N.; Karatsu, T.; Futami, Y.; Kunihiro, T.; Kiyota, A.; Kitamura, A. *Bull. Chem. Soc. Jpn.* **1996**, *69*, 3325–3329. (c) Faria, J. L.; Steenken, S. *J. Am. Chem. Soc.* **1990**, *112*, 1277–1279.

(12) (a) Pirrung, M. C.; Pansare, S. V. *J. Comb. Chem.* **2001**, *3*, 90–96. (b) Borhan, B.; Wilson, J. A.; Gasch, M. J.; Ko, Y.; Kurth, D. M.; Kurth, M. J. *J. Org. Chem.* **1995**, *60*, 7375–7378. (c) Barlos, K.; Gatos, D.; Kallitsis, J.; Papaphotiu, G.; Sotiriu, P.; Wenqing, Y.; Schäfer, W. *Tetrahedron Lett.* **1989**, *30*, 3943–3946.

(13) Bemhardt, S.; Baumgarten, M.; Wagner, M.; Müllen, K. *J. Am. Chem. Soc.* **2005**, *127*, 12392–12399.

(14) (a) Okamoto, Y.; Shimakawa, Y. *J. Org. Chem.* **1970**, *35*, 3752–3756. (b) Katritzky, A. R.; Watson, C. H.; Dega-Szafran, Z.; Eyler, J. R. *J. Am. Chem. Soc.* **1990**, *112*, 2471–2478.

(15) Sahoh, N.; Watanabe, T.; Iketaki, Y.; Omatsu, T.; Fujii, M.; Yamamoto, K. *Polym. Adv. Technol.* **2004**, *15*, 159–163.

(16) Nakajima, R.; Tsuruta, M.; Higuchi, M.; Yamamoto, K. *J. Am. Chem. Soc.* **2004**, *126*, 1630–1631.

(17) Higuchi, M.; Shiki, S.; Ariga, K.; Yamamoto, K. *J. Am. Chem. Soc.* **2001**, *123*, 4414–4420.

(18) Hill, Z. D.; Maccarthy, P. *J. Chem. Educ.* **1986**, *63*, 162.

(19) Fujii, A.; Ochi, Y.; Nakajima, R.; Yamamoto, K. *Chem. Lett.* **2009**, *38*, 418–419.

(20) Yamamoto, K.; Higuchi, M.; Kimoto, A.; Imaoka, T.; Masachika, K. *Bull. Chem. Soc. Jpn.* **2005**, *78*, 349–355.

(21) (a) Döring, S.; Erker, G.; Fröhlich, R.; Meyer, O.; Bergander, K. *Organometallics* **1998**, *17*, 2183–2187. (b) Blackwell, J. M.; Piers, W. E.; Parvez, M.; McDonald, R. *Organometallics* **2002**, *21*, 1400–1407.

(22) (a) Edward, J. *J. Chem. Educ.* **1970**, *47*, 262–270. (b) Zhao, Y. H.; Abraham, M. H.; Zissimos, A. M. *J. Chem. Inf. Comput. Sci.* **2003**, *43*, 1848–1854.
(23) Imaoka, T.; Tanaka, R.; Yamamoto, K. *Chem.—Eur. J.* **2006**, *12*, 7328–7336.
(24) Matos, M. S.; Hofkens, J.; Verheijen, W.; De Schryver, F. C.; Hecht, S.; Pollak, K. W.; Fréchet, J. M. J.; Forier, B.; Dehaen, W. *Macromolecules*. **2000**, *33*, 2967–2973.
(25) Imaoka, T.; Tanaka, R.; Arimoto, S.; Sakai, M.; Fujii, M.; Yamamoto, K. *J. Am. Chem. Soc*. **2005**, *127*, 13896–13905.
(26) Takanashi, K.; Fujii, A.; Nakajima, R.; Chiba, H.; Higuchi, M.; Einaga, Y.; Yamamoto, K. *Bull. Chem. Soc. Jpn*. **2007**, *80*, 1563–1572.
(27) Takanashi, K.; Chiba, H.; Higuchi, M.; Yamamoto, K. *Org. Lett*. **2004**, *6*, 1709–1712.